Placenta 117 (2022) 139–149

Contents lists available at ScienceDirect

Placenta

journal homepage: www.elsevier.com/locate/placenta

Krüppel-like factor 6 (KLF6) requires its amino terminal domain to promote villous trophoblast cell fusion

Andrea L. Miranda [a,b], Ana C. Racca [a,b], Lucille T. Kourdova [a,b], Maria Laura Rojas [a,b], Mariano Cruz Del Puerto [a,b], Gonzalo Rodriguez-Lombardi [a,b], Andrea V. Salas [c], Claudia Travella [c], Elaine.C.O. da Silva [d], Samuel T. de Souza [d], Eduardo.J.S. Fonseca [d], Aldilane. L.X. Marques [e], Alexandre U. Borbely [e], Susana Genti-Raimondi [a,b], Graciela M. Panzetta-Dutari [a,b,*]

[a] Universidad Nacional de Córdoba, Facultad de Ciencias Químicas, Departamento de Bioquímica Clínica, Ciudad Universitaria, X5000HUA, Córdoba, Argentina
[b] Consejo Nacional de Investigaciones Científicas y Tecnológicas (CONICET), Centro de Investigaciones en Bioquímica Clínica e Inmunología (CIBICI), Ciudad Universitaria, X5000HUA, Córdoba, Argentina
[c] Servicio de Ginecología y Obstetricia, Hospital Privado Universitario de Córdoba, X5000HUA, Córdoba, Argentina
[d] Optics and Nanoscopy Group, Physics Institute, Federal University of Alagoas, Maceio, Brazil
[e] Cell Biology Laboratory, Institute of Health and Biological Sciences, Federal University of Alagoas, Maceio, Brazil

ARTICLE INFO

Keywords:
KLF6
Regulatory domain
Villous trophoblast
Differentiation
Cellular elasticity

ABSTRACT

Introduction: Villous cytotrophoblast (vCTB) cells fuse to generate and maintain the syncytiotrophoblast layer required for placental development and function. Krüppel-like factor 6 (KLF6) is a ubiquitous transcription factor with an N-terminal acidic transactivation domain and a C-terminal zinc finger DNA-binding domain. KLF6 is highly expressed in placenta, and it is required for proper placental development. We have demonstrated that KLF6 is necessary for cell fusion in human primary vCTBs, and in the BeWo cell line.

Materials and methods: Full length KLF6 or a mutant lacking its N-terminal domain were expressed in BeWo cells or in primary vCTB cells isolated from human term placentas. Cell fusion, gene and protein expression, and cell proliferation were analyzed. Moreover, Raman spectroscopy and atomic force microscopy (AFM) were used to identify biochemical, topography, and elasticity cellular modifications.

Results: The increase in KLF6, but not the expression of its deleted mutant, is sufficient to trigger cell fusion and to raise the expression of β-hCG, syncytin-1, the chaperone protein 78 regulated by glucose (GRP78), the ATP Binding Cassette Subfamily G Member 2 (ABCG2), and Galectin-1 (Gal-1), all molecules involved in vCTB differentiation. Raman and AFM analysis revealed that KLF6 reduces NADH level and increases cell Young's modulus. KLF6-induced differentiation correlates with p21 upregulation and decreased cell proliferation. Remarkable, p21 silencing reduces cell fusion triggered by KLF6 and the KLF6 mutant impairs syncytialization and decreases syncytin-1 and β-hCG expression.

Discussion: KLF6 induces syncytialization through a mechanism that involves its regulatory transcriptional domain in a p21-dependent manner.

1. Introduction

Villous cytotrophoblast (vCTB) differentiation into the syncytiotrophoblast (STB) layer implies two related events. One, characterized by cell aggregation, merging of plasma membranes with mixing of cell contents termed morphological differentiation, and other characterized by the expression of genes involved in hormone synthesis, and substrate transport, among others, known as the biochemical differentiation. STB is maintained by the continuous fusion of vCTBs with the overlying syncytium in a regenerative process [1]. The multinucleated syncytium protects the fetus from exposure to harmful materials and it is the primary site for maternal-fetal exchange of nutrients, gases, and waste

* Corresponding author. Departamento de Bioquímica Clínica, (CIBICI) CONICET Facultad de Ciencias Químicas, Universidad Nacional de Córdoba, Ciudad Universitaria, X5000HUA, Córdoba, Argentina.
E-mail addresses: gpan@fcq.unc.edu.ar, gmpanzetta@unc.edu.ar (G.M. Panzetta-Dutari).

https://doi.org/10.1016/j.placenta.2021.12.006
Received 18 August 2021; Received in revised form 11 November 2021; Accepted 1 December 2021
Available online 4 December 2021

products, and for the synthesis of important pregnancy-associated proteins. Impaired STB differentiation, renewal, or function are associated with preeclampsia, the principal cause of maternal morbidity and mortality, and with other pregnancy-associated disorders including chronic disease in the adult life of the offspring [2–5].

Various signaling pathways, proteins, growth factors, cytokines, as well as extracellular matrix components and mechanical forces are involved in the syncytialization process [1,6,7]. Among them, the two fusogenic membrane glycoproteins, syncytin-1 and syncytin-2, play a major role [8–10]. Human chorionic gonadotrophin (hCG), composed of the specific β-subunit and a common α-subunit, as well as its hyperglycosylated variant display several paracrine-autocrine functions essential for pregnancy including syncytium formation and renewal [11,12]. Other proteins involved in biochemical and/or morphological differentiation of the villous trophoblast include GRP78, the endogenous and xenobiotic substrate transporter ABCG2, and Gal-1, a soluble member of the mammalian β-galactoside-binding proteins [13–16]. KLF6 is one of the transcription factors that have a demonstrated or suggested function in the syncytialization process [17,18]. KLF6 is highly expressed in placenta and *Klf6*$^{-/-}$ mice die at day E12.5 showing impaired placental development [19,20]. We have previously demonstrated that KLF6 is present throughout the *in vitro* differentiation of human vCTB with an early and transient increase in its expression before syncytium formation. In addition, it transactivates promoter constructs of the chorionic gonadotropin subunit beta 5 (*CGB5*), *PSG3*, and *PSG5* genes [21]. KLF6 knockdown impairs cell-cell fusion and reduces the expression of genes encoding syncytin-1 and p21, its overexpression leads to increased transcript levels of the genes encoding hCG, PSG, syncytin-1, syncytin-2, connexin 43 (Cx43) and zona occludens (ZO-1) in the JEG-3 cell line, as well as those for Syn-2 and Cx43 in CTB cells undergoing spontaneous *in vitro* syncytialization [21,22]. However, whether KLF6 triggers human trophoblast cell-cell fusion, and which is the mechanism involved remain unknown. Herein, BeWo choriocarcinoma cell line, a standard model to mimic syncytialization of human placental villous trophoblast, and cultures of human placental vCTBs, were used as *in vitro* systems to evaluate whether increased KLF6 expression induces cell-cell fusion and to address the implicated mechanism.

2. Materials and methods

2.1. Placenta collection, cytotrophoblast isolation, and cell culture and differentiation

Human placentas were obtained after cesarean sections from mothers with uncomplicated pregnancies. The study was performed with the ethics approval of the local Advisory Committee of Biomedical Research in Humans, Córdoba, Argentina (RePIS No. 1202, HP 4-112), and written informed consent was required. Placentas were processed within 30 min after delivery and vCTB cells were purified, cultured, and differentiated as previously described [22].

BeWo (ATCC No. CCL98) cell line and BeWo cells stably transfected with expression vectors carrying the full length KLF6 (KLF6-B), the amino-terminal deleted KLF6 mutant (KΔac-B), or with the empty cloning vector (EV-B) were grown in DMEM-F12 (Invitrogen) supplemented with antibiotics (100 U/mL penicillin/0.1 mg/mL streptomycin) and 10% (v/v) FBS (Internegocios S.A).

2.2. Lentiviral plasmid constructs

The pLenti-KLF6 plasmid, containing the human *KLF6* (NM_001300) full-length cDNA sequence (852 bp), and pLenti-KΔac plasmid, lacking the sequence encoding for the first 103 amino acids, were constructed. The *KLF6* sequences were amplified from the pXJ-KLF6 recombinant plasmid [23] and subcloned into the BamHI/XbaI cloning sites of the pLenti CMV/TO puro empty (w175-1) expression vector (Addgene #17482). Construct identities were verified by DNA sequencing (Macrogen, Korea).

2.3. Generation of stable transfected cells and transduction of BeWo and vCTB

pLenti-KLF6, pLenti-KΔac, and pLenti CMV/TO puro empty vector (pLenti-EV) were cotransfected with pMD2.G and psPAX2 vectors in 293T cells using Jet Prime (Polypus Transfection) according to the manufacturer protocol. Viral supernatants were collected 48 and 72 h later. BeWo cells (2×10^5 cells/well) plated in 6-well plates were transduced with 50% (v/v) viral supernatants supplemented with 8 μg/mL polybrene (Sigma-Aldrich). Twenty-four hours later, cells were washed and cultured for 24 h in fresh supplemented culture medium. Stable transfected KLF6-B, KΔac-B, and EV-B cells were selected with 2 μg/mL of puromycin (Sigma-Aldrich) for 2 weeks. All the experiments were performed with stable BeWo cells with less than 5 passages.

Placental purified vCTBs (1.8×10^5 cells/well) were washed twice with PBS 4 h after plating and transduced with pLenti-KLF6, pLenti-KΔac, or pLenti-EV as described above.

2.4. Small interfering RNA transfections

KLF6-B cells (1.5×10^5 cells/well) seeded in 6-well plates were cultured for 24 h and transfected with 25 nM of *KLF6*-specific small interfering RNA (siK) (Ambion Silencer Select siRNA, ID # 9700, ThermoFisher) (sense 5′-GGAAGAUCUGUGGACCAAAtt-3′, antisense 5′-UUUGGUCCACAGAUCUUCCtg-3′) or 50 nM of p21-specific small interfering RNA (sip21) (Sigma-Aldrich, ID # 870; SASI_Hs01 00025256) or with the control scrambled siRNA (SCR) (Ambion Silencer Negative Control #1 siRNA, ThermoFisher) using 4 μL of Lipofectamine RNAiMAX reagent (Invitrogen) in 1 mL of serum and antibiotic-free OPTI-MEM. Four hours later, 1 mL of DMEM-F12 supplemented medium was added and cells analyzed 72 h later.

2.5. Cell fusion and immunofluorescence assays

Wild type or stably transfected BeWo cells were seeded in a 6-well plate (1.5×10^5 cells/well) in DMEM-F12 supplemented medium. Freshly purified vCTB cells were seeded in 96-well plates (1.8×10^5 cells/well) in KGM supplemented culture medium and transduced with the lentiviral particles. Cell fusion was evaluated after 72 h, unless indicated.

Immunofluorescence assays were performed as previously described [21] with mouse anti-desmoplakin (1:100; ab16434, Abcam Co.) and mouse monoclonal anti-cytokeratin 7 (Clone OV-TL 12/30, N1626, Dako) primary antibodies, and Alexa Fluor 594-conjugated F(ab)2-goat anti-mousse IgG (A11020, ThermoFisher) as the species-specific secondary antibody in a 1:720 final dilution. Nuclei were counterstained with Hoechst 33342 dye (Molecular Probes, Cat. H-21492). Slides were mounted in aqueous mounting media (Mowiol 4-88, Sigma Aldrich) and images were recorded using Leica DMI8 microscope equipped with LASX software or Nikon optical microscope with NIS software (Nikon eclipse TE2000-U, USA). The number of syncytia, nuclei in syncytia, and total nuclei from at least 7 randomly chosen microscopic fields for each condition were counted using FIJI software. Fusion index was calculated as (N-S)/T, where N is the number of nuclei in the syncytia, S the number of syncytia, and T the total number of nuclei.

2.6. Cell flow cytometry

Cells were detached with trypsin-EDTA 0.05% (w/v) (ThermoFisher), trypsin was inactivated with DMEM-F12 supplemented medium plus 5 mM EDTA (final concentration), cells were fixed with 2% (w/v) paraformaldehyde 2% (w/v) sucrose for 15 min and maintained at 4 °C until analysis by flow cytometry using a BD FACS Canto II cytometer (BD

Table 1
Oligonucleotides used for qRT-PCR assays.

Transcript	Primer name	Sequence (5′-3′)	Conc.(nM)
Syncytin-1	ERVW1-F	GCAACCACGAACGGACATC	200
	ERVW1-R	GTATCCAAGACTCCACTCCAGC	
ABCG2	ABCG2-F	CAATGGGATCATGAAACCTG	250
	ABCG2-R	CATTTATCAGAACATCTCCAGA	
Gal1	Gal1-F	CCTGGAGAGTGCCTTCGAGTG	400
	Gal1-R	CTGCAACACTTCCAGGCTGG	
Cx43	Cx43-F	ACTTGCCTTTTCATTTTACTTC	200
	Cx43-R	CCTGGGCACCACTCTTTT	
PPIA	PPIA-F	GTTTTGCAGACGCCACCG	100
	PPIA-R	GCAAACAGCTCAAAGGAGACG	

Biosciences). A total of 40000 events per analysis were collected. The data were analyzed by FlowJo vX.0.7 software as described in Ref. [24].

2.7. Western blotting

Total protein samples, separated on a 10% or 14% (w/v) SDS–PAGE, were transferred to a Hybond-ECL nitrocellulose (GE Healthcare) as previously described [21]. Antibodies used were: mouse monoclonal anti-KLF6 (1:1000; 2c11) whose specificity was previously determined [25], mouse monoclonal anti-α-tubulin (1:3000; T9026, Sigma-Aldrich), rabbit polyclonal anti-KLF6 (1:50; R-173, Santa Cruz Biotechnology), rabbit polyclonal anti-syncytin-1 (1:500; z-25, Santa Cruz Biotechnology), rabbit monoclonal anti-p21 (1:1000, Cell Signaling), rabbit polyclonal anti-β-hCG (1:500; A0231, Dako), rabbit polyclonal anti-GRP78 (1:1000, Cell Signaling) and mouse monoclonal anti-β-actin (1:1000; A2228, Sigma-Aldrich). After washing, blots were revealed with IRDye 800CW donkey anti-rabbit IgG (Li-Cor Biosciences, cat no: 926-32213), IRDye 680RD donkey anti-mouse IgG (Li-Cor Biosciences, cat no: 926-68072) or IRDye 800CW Donkey anti-mouse IgG (Li-Cor Biosciences, cat no: 926-32212) secondary antibodies (1:10000). Membranes were visualized and quantified using the Odyssey Infrared Imaging System (LI-COR, Inc) and the Image Studio software.

2.8. Real-time quantitative RT-PCR (qRT-PCR)

RNA purification, cDNA synthesis, primer design, qRT-PCR quantification, amplification efficiency, and specificity were performed and/or calculated as described in Ref. [22]. Primer sequences and concentrations are indicated in Table 1.

2.9. Proliferation assays

Cell proliferation was evaluated by bromodeoxyuridine (BrdU, B5002, Sigma-Aldrich) incorporation into DNA during its synthesis as previously described [26]. Cells were cultured for 72 h and incubated

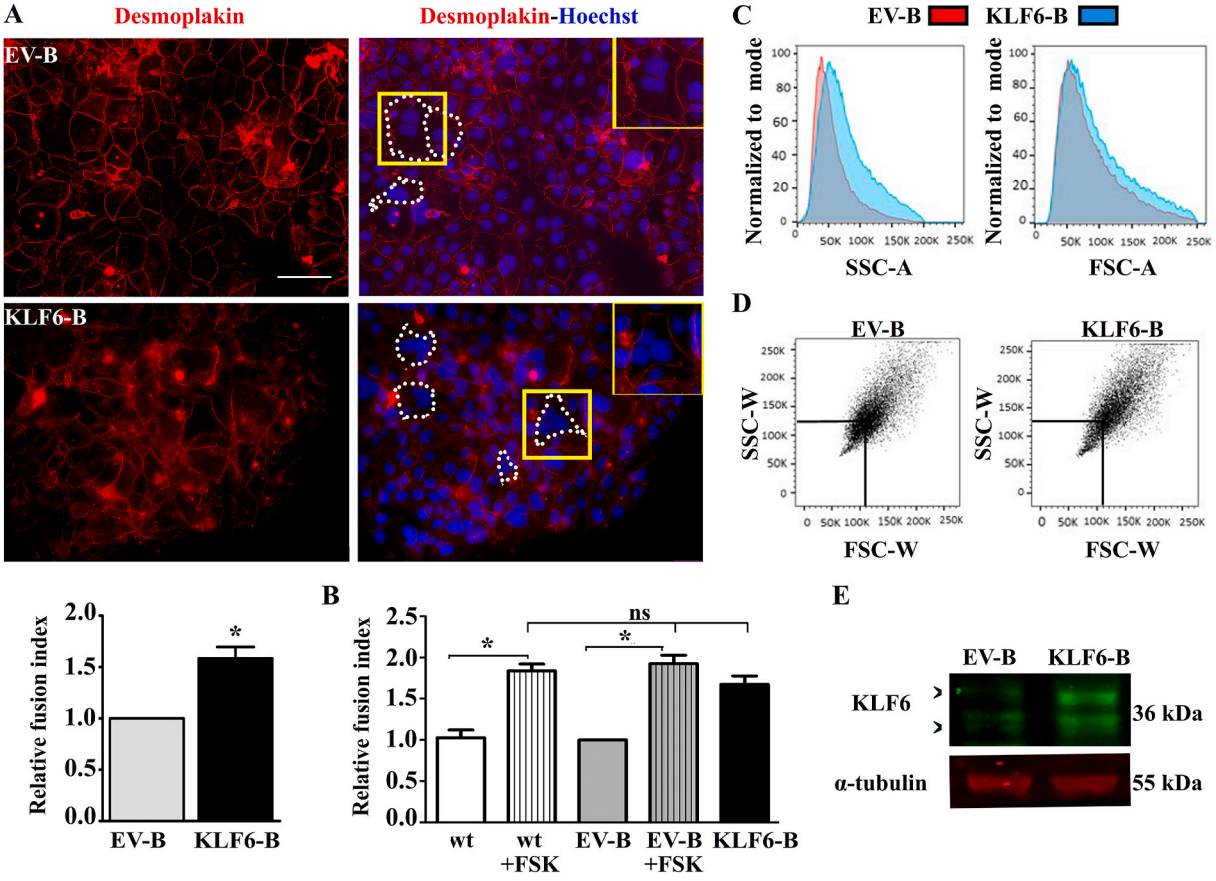

Fig. 1. KLF6 promotes BeWo cell-cell fusion. **A**- KLF6-B and EV-B cells immunostained with desmoplakin and nuclei counterstained with Hoechst. White dotted lines demarcate syncytial-like structures. The insets show a magnified image of the boxed regions in the main panels. Scale bar = 100 μm. The bar graph represents the relative fusion index in KLF6-B setting spontaneous fusion of EV-B cells as 1 (mean ± SEM, *p < 0.05, one sample *t*-test, n = 3). **B**- Fusion index of wild-type (wt) and EV-B cells treated or not with forskolin (FSK), as well as KLF6-B relative to the fusion observed in EV-B. Cells were seeded in 96-well plates (5×10^3 cells/well), treated or not with 30 μM FSK to induce fusion for 72 h and fusion index was analyzed by immunofluorescence. The mean ± SEM is shown (*p < 0.05, ANOVA, post-test Tukey's multiple comparison, ns: not significant, n = 3). **C**- Flow cell cytometry analysis of KLF6-B (blue) and EV-B (red) cell granularity and size determined by side-scatter area (SSC-A) and forward-scatter area (FSC-A). **D**- Side-scatter width (SSC-W) plotted against forward-scatter width (FSC-W) of KLF6-B and EV-B cells. **E**- Western blot analysis of KLF6 in KLF6-B and EV-B cells, α-tubulin was included as loading control and one representative blot is shown. (For interpretation of the references to colour in this figure legend, the reader is referred to the Web version of this article.)

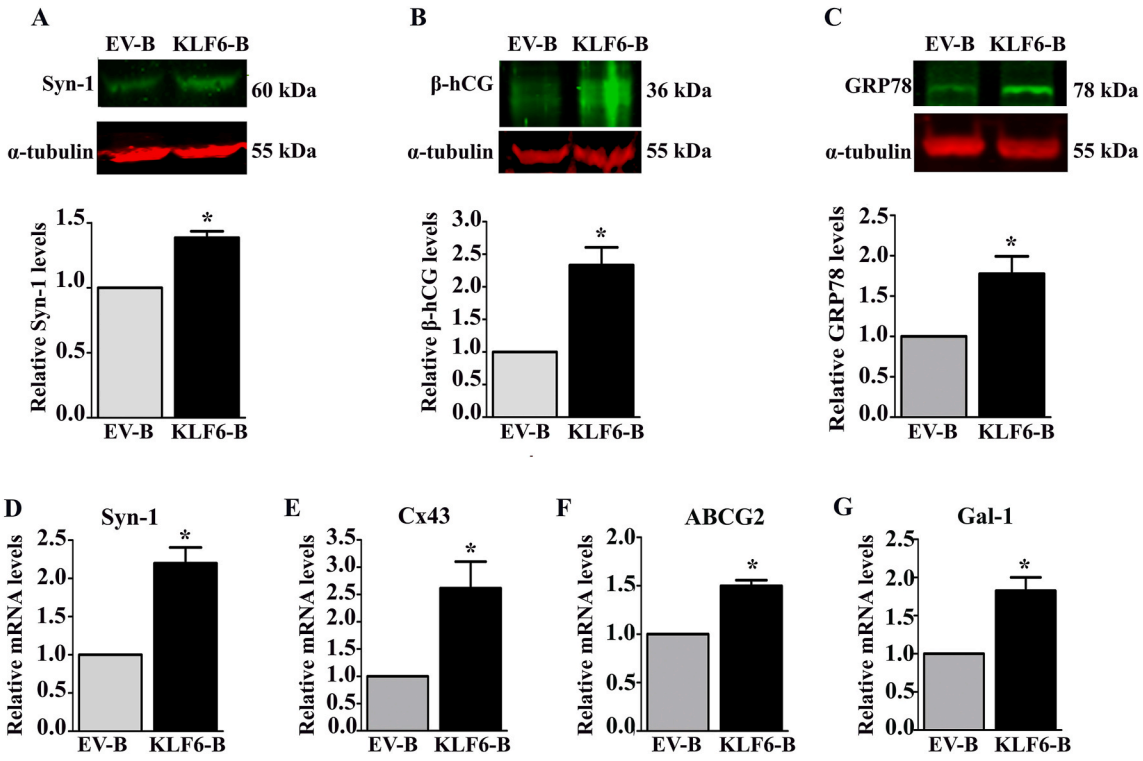

Fig. 2. KLF6 upregulates the expression of molecules involved in vCTB differentiation. Representative WB images for syncytin-1 (Syn-1) (**A**), β-hCG (**B**), and GRP78 (**C**) proteins in KLF6-B and in EV-B cells, α-tubulin was used as loading control. Bar graphs show the densitometric quantification of protein levels normalized to the α-tubulin signal and expressed relative to the control condition in each experiment. The bars represent the mean ± SEM (*$p < 0.05$, one sample *t*-test, n = 3). Transcript levels of Syn-1 (**D**), Cx43 (**E**), ABCG2 (**F**) and Gal-1 (**G**) were determined by qRT-PCR from total RNA. Bars represent the mean ± SEM of the relative level of each transcript in KLF6-B normalized to cyclophilin A with respect to the control condition (EV-B) (*$p < 0.05$, one sample *t*-test, n = 3).

with 20 μM BrdU for the last 4 h.

2.10. Cell fusion evaluated through atomic force microscopy (AFM)

BeWo cells (2×10^5 cells/well) plated over glass coverslips were transiently transduced with the pLenti-EV or pLenti-KLF6. Seventy-two hours later, cells were PBS-washed and fixed with 0.5% glutaraldehyde in PBS (v/v) for 5 min, washed again and dried at room temperature. Cellular morphology images and elasticity measurements were obtained using a standard AFM setup as described in Ref. [27]. Cell topography was imaged (256 × 256 pixels) in tapping mode with a scan rate of 0.3–1 Hz. The AFM experiments were performed, images processed, and local mean Young's modulus calculated as described in Ref. [27], except that the maximum indenting force for the cantilever was set at 30 nN. Force-displacement curves of 50 random cells from three different experiments were acquired for each group of cells.

2.11. Raman spectroscopy measurements and data analysis

BeWo cells were processed and fixed as described for AFM. Raman spectra were measured on mononuclear cells or syncytium-like structures in the spectral range of 600–1800 cm^{-1}. Raman spectra were obtained using a XploRA spectrometer (Horiba, Japan) coupled to an optical microscope (BXFM, Olympus, Japan) and equipped with a 532 nm laser that was focused on the cell nucleus through a 60× oil immersion objective (NA = 1.4). The frequency calibration was established by reference to the vibratory band of 520 cm^{-1} of a silicon sheet. A 785 nm diode laser that operated at 113 mW/line was used for excitation. A low power irradiation at the sample surface was used, around 5 mW (3s laser exposure for 5 accumulations). The diffraction grating was 1200 lines/mm and yielded a spectral resolution of 1.5 cm^{-1}. All spectra were smoothed, background-adjusted, and normalized using an algorithm implemented in MatLab software, before conducting the spectral analysis (Mathworks, Naticks, MA, USA), to suppress the external noises and enhance the useful information about the biochemical composition. Principal Component Analysis (PCA) was performed to evaluate the spectral variability in the dataset. Each cell group was subjected to 2D- and 3D-PCA.

2.12. Statistical analysis

Comparisons between groups were performed using the Student's t-test or Mann-Whitney test. One-way analysis of variance (ANOVA) with a Tukey's or Dunnett's post-test was performed for multiple comparisons. A one-sample *t*-test was used to determine whether values were significantly different from the control value set as 1. Multivariate statistical analyses were implemented in MatLab software. Statistical analyses were performed using the GraphPad Prism 5.0 software. A probability value of $p < 0.05$ was considered statistically significant.

3. Results

3.1. KLF6 promotes BeWo cell-cell fusion

To prove whether KLF6 overexpression promotes human trophoblast cell-cell fusion we first analyzed the effect of KLF6 on the morphological differentiation of BeWo cells, a useful cell model to study molecular aspects of human placental trophoblast syncytialization [18]. Cells stably transformed with KLF6 or the empty vector (KLF6-B and EV-B, respectively) were immunostained with anti-desmoplakin and with Hoechst. Immunofluorescence microscopy revealed an increase in the relative fusion index of KLF6-B compared to EV-B cells (Fig. 1A). KLF6-B fusion was comparable to that observed in wild type or EV-B cells treated with 30 μM forskolin for 72 h (Fig. 1B). Morphological differentiation

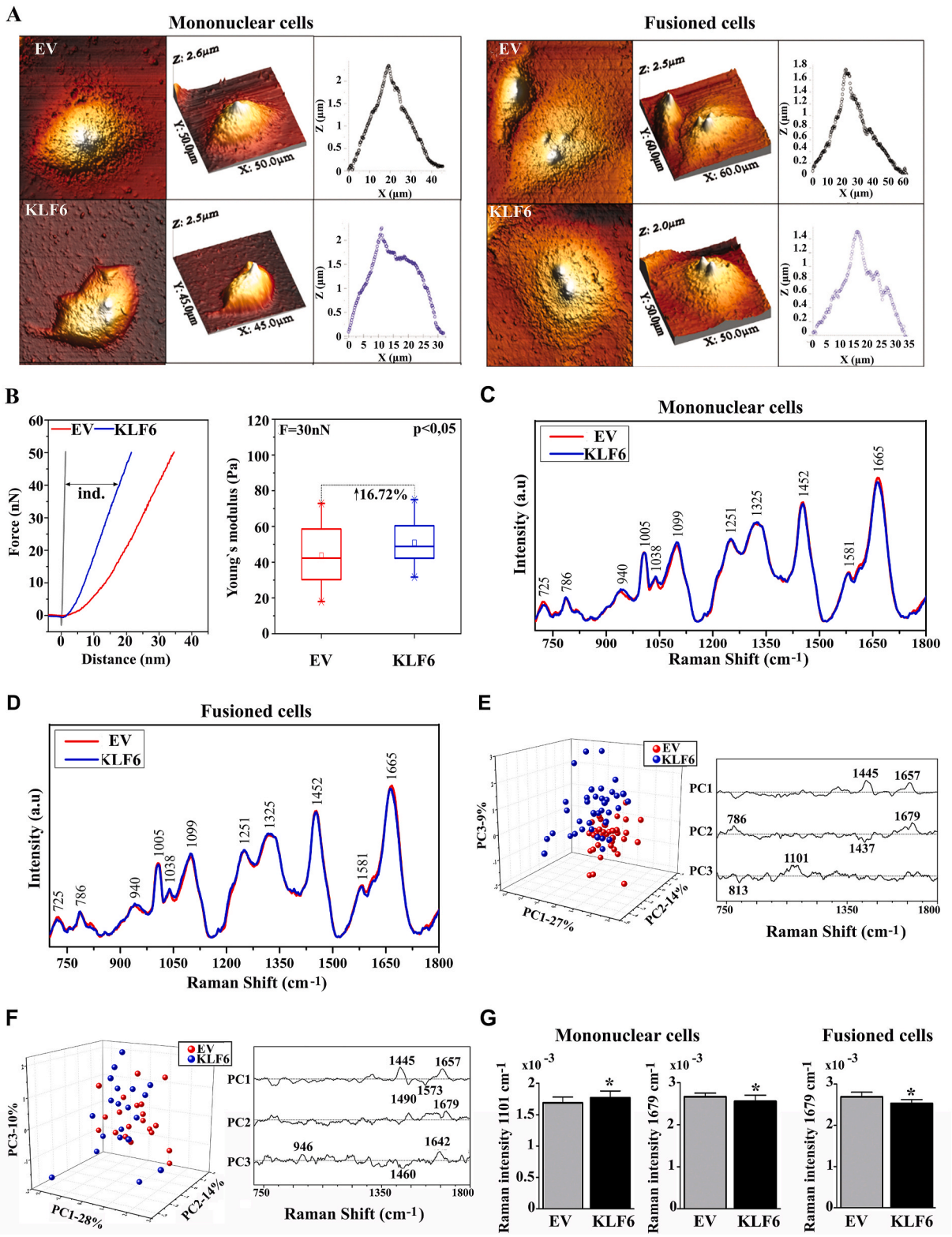

Fig. 3. KLF6 changes topography, elasticity and generates biochemical modifications in BeWo cells. Mononuclear or fused BeWo cells transiently transduced with pLenti-KLF6 or pLenti-EV were analyzed by AFM and Raman spectroscopy. **A**- Representative three-dimensional AFM images and the height profiles from mononuclear (left panel) and fused cells (right panel). **B**- Media of force-displacement curves and Young's modulus measured in 50 cells of each type. The gray vertical line in the force-displacement graph represents the reference stiff glass surface. Ind: indentation. **C**- Average Raman spectra of 40 mononuclear cells of each condition. **D**- Average Raman spectra of 20 fused cells of each type. **E**- PCA and PC loadings from mononuclear cells. The first three PC explained 50% of the variance of the original data set. The contribution of each PC is shown in the figure. **F**- PCA and PC loadings from fused cells. The first three PC explained 52% of the variance of the original data set. The contribution of each PC is shown in the figure. **G**- Raman intensity of individual peaks that showed significant difference in mononuclear (1101 and 1679 cm^{-1}) and fused (1679 cm^{-1}) cells. Mean ± SEM, (*$p < 0.05$, Mann-Whitney test).

was also demonstrated by cell flow cytometry analysis revealing higher granularity and size in KLF6-B than in EV-B cells (Fig. 1C), consistent with cell fusion [28,29]. In addition, KLF6-B cell population showed a linear increase in side-scatter width (SSC-W) *versus* forward-scatter width (FSC-W) as compared to EV-B cells (Fig. 1D), confirming an increase in cell fusion [24,30]. Western blot assays verified KLF6 overexpression (Fig. 1E) detected as a double band corresponding to the hyper and hypophosphorylated forms as previously described [23].

Fusion index increase was likewise observed in BeWo cells transiently transduced with pLenti-KLF6 compared to cells transduced with pLenti-EV (Supplemental Fig. 1A). Moreover, downregulation of *KLF6* expression in KLF6-B cells with a specific siRNA against *KLF6* (siK) abrogated the increase in cell fusion, revealing that morphological differentiation is specifically related to the overexpression of KLF6. EV-B and wild type cells showed similar basal fusion index, indicating that transformation with the empty vector does not alter BeWo's cell fusion (Supplemental Fig. 1B). These results indicate that KLF6 overexpression increases spontaneous BeWo cell fusion and suggest that KLF6 promotes trophoblast syncytialization.

3.2. KLF6 upregulates the expression of molecules involved in trophoblast syncytialization

In agreement with the increase in cell fusion, syncytin-1 protein and transcript were higher in KLF6-B compared to EV-B cells (Fig. 2A&D). Moreover, β-hCG (Fig. 2B) and GRP78 (Fig. 2C) protein levels as well as transcripts coding for Cx43, ABCG2 and Gal-1 were also upregulated (Fig. 2E–G). These results indicate that KLF6 enhances the expression of molecules involved in STB differentiation.

3.3. KLF6 changes topography, elasticity, and generates biochemical modifications in BeWo cells

AFM, a non-invasive, label free, high-resolution imaging technique, was used to compare cell surface topography and biomechanical elasticity between BeWo cells transiently transduced with pLenti-KLF6 or with the control pLenti-EV. Mononuclear cells in the KLF6 group were more elongated than in the control condition, while fused cells were morphologically similar in both conditions presenting as large cells with prominent nucleoli (Fig. 3A). The biomechanical elasticity through cell indentation was analyzed without discrimination between mononuclear and fused cells. Quantification of Young's modulus revealed a 16.72% increase in the KLF6 group compared to EV ($p < 0.05$), which represents increased stiffness (Fig. 3B).

Raman spectroscopy was employed as a novel approach to explore BeWo cellular biochemical modifications induced by KLF6 overexpression. The average spectra from 40 mononuclear (Fig. 3C) and 20 fused cells (Fig. 3D) from the EV and KLF6 groups were recorded and analyzed. Principal component analysis (PCA) was used for classification of the different groups and interpretation of the spectral data. Three-dimensional plots constructed with combinations of sets of scores of the first three PCs as well as plots of the PC1, PC2 and PC3 loadings are shown (Fig. 3E&F). This information was used for the determination of the differentiation capability of PCA and the identification of significant Raman features. Regarding the PCA from mononuclear cells, the first three PC explained 50% of the variance of the original data set, and based on the PCA mixed distribution, mononuclear cells from the KLF6 and EV groups could be distinguished amid each other, indicating significant variability between them (Fig. 3E). Regarding the PCA of fused cells the first three PC explained 52% of the variance of the original data set, although the PCA mixed distribution showed the KLF6 and EV groups cannot be characterized as different (Fig. 3F). Mononuclear cell loadings indicated positive correlation of Raman bands at 1445, 1657, 786, 1679, and 1101 cm^{-1}, and negative correlation at 1437 and 813 cm^{-1} (Fig. 3E). Fused cell loadings showed positive correlations at 1445, 1657, 1490, 1679, 946, 1642, and 1756 cm^{-1}, and negative at 1490, 1573 and 1460 cm^{-1} (Fig. 3F). Raman band assignments of the most prominent variances identified by PCA were supported on published literature and used for spectral features interpretation (Table 2) [31–36]. Only two peaks had significant intensity differences between mononuclear cells of the KLF6 and EV groups. The 1101 cm^{-1} peak, assigned to O-P-O backbone stretch from A-DNA, was increased in the KLF6 group ($p < 0.036$), while the 1679 cm^{-1} peak, assigned to C═O stretch with two contributors NADH and amide I, had reduced intensity in the KLF6 group ($p < 0.0008$). This peak was also reduced in fused cells of the KLF6 group ($p < 0.0001$). Indeed, it was the only peak with statistically different intensity found in the analysis of fused cells (Fig. 3G).

Table 2
Raman band assignments.

Raman peak position [cm^{-1}]	Band Assignment	Contributions
725	Ring breathing modes	Adenine
786	O-P-O backbone	DNA
813	C5′- O-P-O - C3′ phosphodiester band	RNA
940	υ(C-C)	Polysaccharides
946	δoop(C–OH) [COOH]	Hyaluronan (sugar-specific)
1005	Ring breathing modes	Phenylalanine
1038	υ(C-N)	Fatty acids, Polysaccharides
1099	PO_2	Nucleotides backbone
1101	O-P-O backbone stretch	DNA
1251	NH_2	Guanine, Cytosine
1325	ωCH_3CH_2	Purines, CoA
1437	αCH_3, αCH_2	Fatty acids, Sphingomyelin
1445	δCH_2, δCH_3	Proteins, Fatty acids
1452	δCH_2, δCH_3	Valine, Proteins
1460	δCH_2, δCH_3	Lipids
1490	δN-H	DNA, Amide II
1573	Ring breathing modes	Adenine, Guanine
1581	υ(C-C)	Phenylalanine
1642	$\beta(NH_3)$	Amide I
1657	υ(C═C)	Membrane lipids (Phosphatydylethanolamine and Phosphatydylcholine), Fumarate
1665	υ_s(C═O)	Amide I (β-sheet)
1679	υ(C═O)	NADH, Amide I
1756	υ(C═O)	Cortisone

α-scissoring, β-bending, δ-deformation, oop-out of plane, τ-twisting, ω-wagging, υ-stretching, υ_s- symmetric stretching.

3.4. KLF6 decreases BeWo cell proliferation and promotes their fusion in a p21-dependent manner

Trophoblast differentiation has been associated with cell cycle arrest and upregulation of p21 expression [37], and KLF6 inhibits cellular growth in different cell contexts in part activating p21 [38,39]. Therefore, we hypothesized that KLF6 overexpression could reduce cell proliferation by upregulating p21. Indeed, incorporation of BrdU into newly synthesized DNA was reduced and p21 protein expression was increased in KLF6-B compared to EV-B cells (Fig. 4A&B). Moreover, when p21 expression was silenced in KLF6-B cells (Fig. 4C) the formation of syncytium-like structures was reduced compared to KLF6-B cells transfected with the control SCR siRNA (Fig. 4D&E). These results suggest that KLF6 reduces cell proliferation and promotes BeWo cell fusion, at least in part, by upregulating p21.

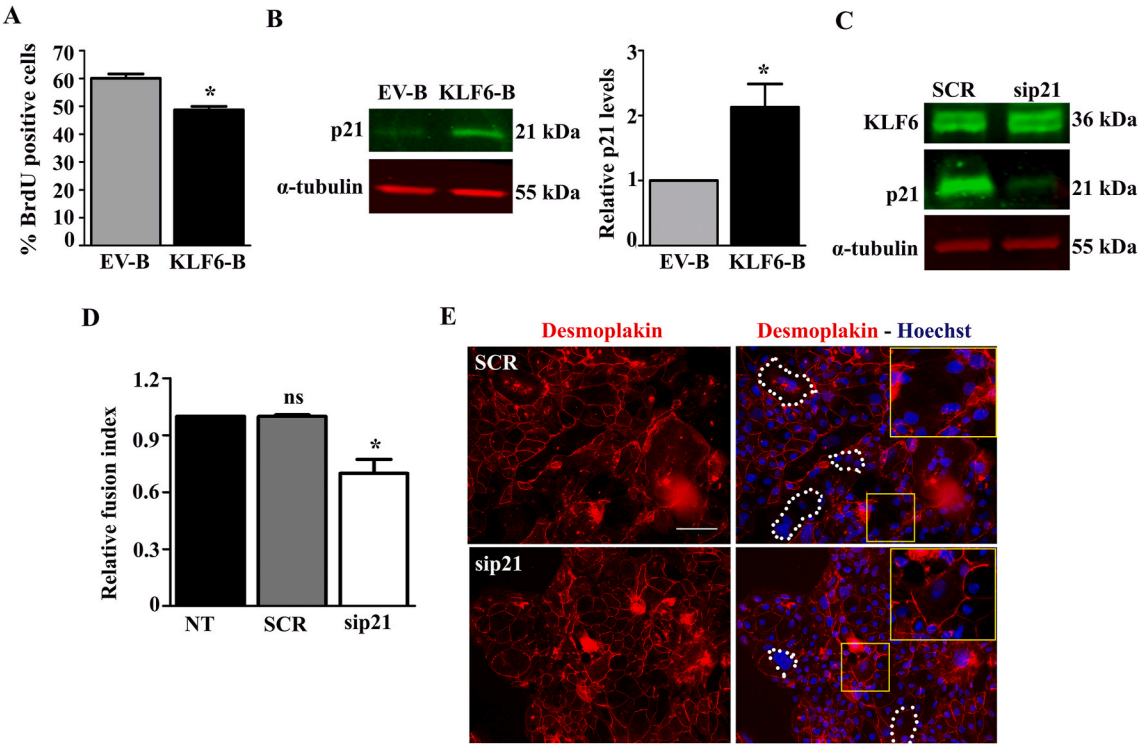

Fig. 4. KLF6 decreases BeWo cell proliferation and promotes their differentiation in a p21-dependent manner. **A-** Percentage of BrdU positive cells in each condition expressed as the mean ± SEM (*p < 0.05, *t*-test, n = 2). For each condition, at least 1000 cells from randomly selected fields were counted. **B-** Representative western blot images for p21 and α-tubulin in KLF6-B and EV-B cells. Bar graphs represent p21 expression level in KLF6-B relative to EV-B defined as 1. Values are expressed as the mean ± SEM (*p < 0.05, one sample *t*-test, n = 3). **C-** Western blot analysis of p21 and KLF6 proteins in KLF6-B cells transfected with a specific siRNA for p21 (sip21) or with the scramble sequence (SCR), α-tubulin was included as loading control. **D-** Fusion index of KLF6-B cells transfected with sip21, SCR, or non-transfected cells expressed relative to the fusion induced in KLF6-B defined as 1. The mean ± SEM is shown (*p < 0.05, ANOVA, post-test Tukey's multiple comparison, ns: not significant, n = 3). **E-** Representative images of desmoplakin immunodetection and nuclei staining with Hoechst of KLF6-B cells transfected with SCR or sip21. White dotted lines demarcate syncytial-like structures. Scale bar = 100 μm. The insets show a magnified image of the boxed regions.

3.5. The N-terminal acidic domain of KLF6 is necessary for BeWo cell fusion

We next evaluated the importance of the N-terminal acidic domain of KLF6 in BeWo cell fusion. As shown in Fig. 5A, KLF6 has a C-terminal Zn-finger DNA-binding domain and a N-terminal domain, rich in acidic amino acids, regarded as the transcription regulatory domain [19,40,41]. BeWo cells were stably transfected with the pLenti-KΔac construct lacking the N-terminal domain (Fig. 5A) and cell differentiation was analyzed. Syncytium-like structures were not increased in KΔac-B, instead fusion index was slightly downregulated compared to EV-B cells, suggesting that KΔac interferes with basal spontaneous cell fusion (Fig. 5B). Accordingly, protein levels of β-hCG and syncytin-1 were reduced (Fig. 5C). Moreover, cell fusion in KLF6-B was diminished when they were transiently transduced with pLenti-KΔac, although high levels of the full-length KLF6 were maintained (Fig. 5D). These results suggest that KLF6 requires its N-terminal domain to promote cell fusion by activating or repressing the expression of target genes. Since the KΔac mutant conserves the DNA-binding domain it seemingly behaves as a negative dominant of KLF6 that interferes with KLF6 function, since it can bind to consensus sequences in target genes but cannot regulate them.

3.6. The N-terminal acidic domain of KLF6 is required for vCTB syncytialization

Despite BeWo cell line is the most widely used cell model to study vCTB differentiation they are derived from choriocarcinoma and may not be fully representative of normal human trophoblasts. Instead, vCTBs isolated from placental tissue better reproduce what occurs in the placenta *in vivo* [18].

To confirm the role of KLF6 on syncytialization, vCTB from normal human term placentas were transduced with KΔac, KLF6, or EV lentivirus particles and cell fusion as well as protein expression were evaluated. As expected, untreated vCTB cells fuse into large syncytium-like structures when they were cultured in serum-containing media. Cell fusion was similar in cells transduced with the EV lentivirus, instead larger syncytium-like structures appeared in cells transduced with KLF6 and decreased in vCTB transduced with the KΔac construct (Fig. 6A). Fusion index quantification in each condition revealed a small but significant increase upon KLF6 overexpression and confirmed that KΔac impairs cell fusion (Fig. 6B). Syncytin-1 was undetectable in early cultures of untreated vCTB but was detected in all the experimental conditions after 72 h. Its expression level was slightly higher in CTBs overexpressing KLF6 and lower in CTBs expressing the KΔac mutant compared to EV-CTB cells (Fig. 6C). Western blot assay verified KLF6 and KΔac expression (Fig. 6D). These results reveal that KLF6 enhances vCTB *in vitro* differentiation through a regulatory mechanism that requires its N-terminal domain.

4. Discussion

Herein, we show that increased KLF6 expression triggers the differentiation of BeWo cells and increases primary human vCTB fusion *in vitro*. This is supported by the fact that KLF6 overexpression in BeWo cells leads to an increase of transcript and/or protein of syncytin-1, β-hCG, GRP78, Cx43, ABCG2, and Gal-1. Moreover, vCTB KLF6-induced fusion correlates with a rise in syncytin-1 protein levels. Present results further extend those previously reported [22]. Altogether, they demonstrate that KLF6 promotes the expression of proteins that

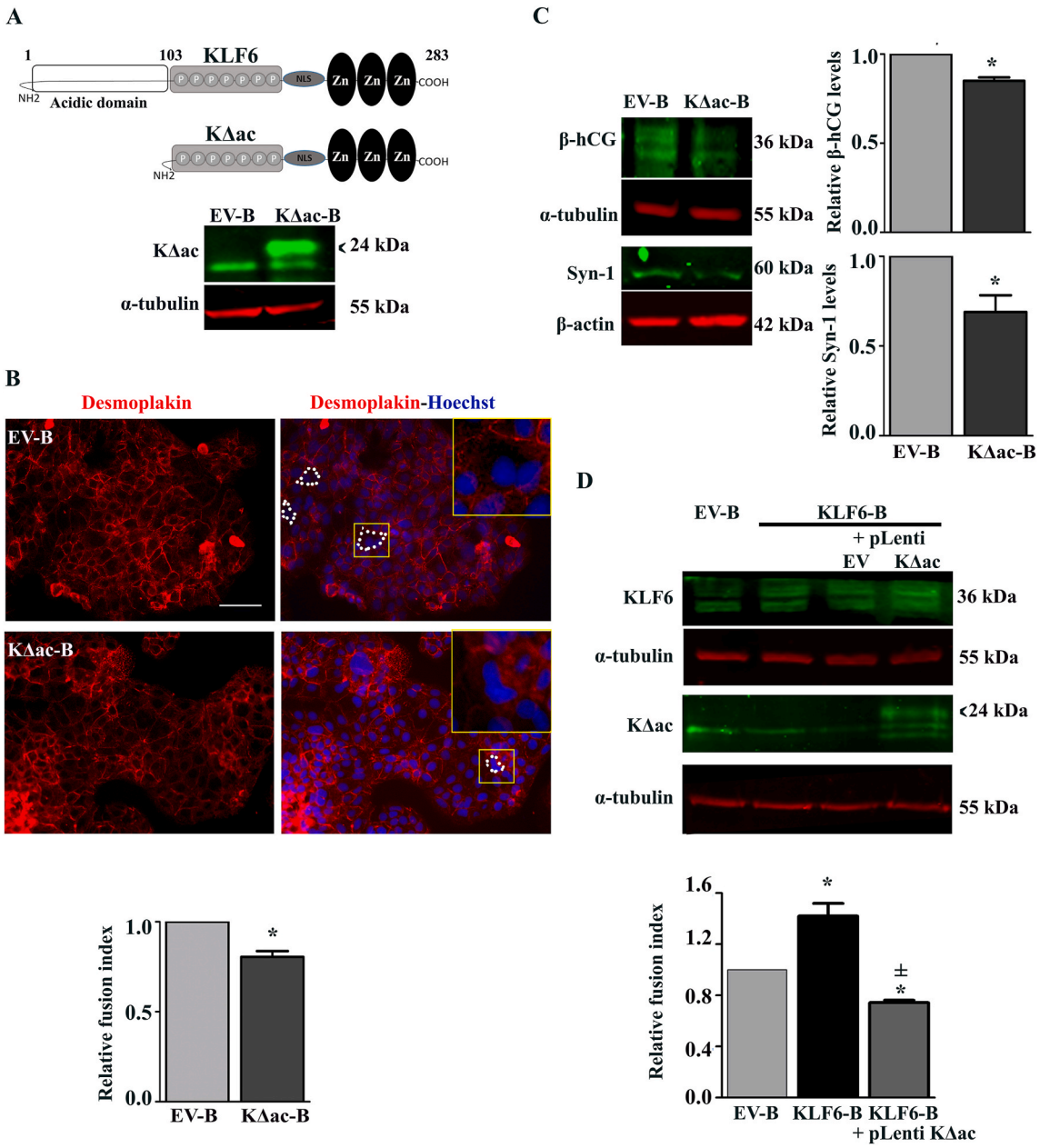

Fig. 5. The N-terminal acidic domain of KLF6 is required for BeWo cell differentiation. **A**- Schematic representation of KLF6 N-terminal deletion mutant (KΔac). The numbers on the top of the scheme indicate the amino acid positions. A representative western blot with the expression of KΔac and α-tubulin as loading control in EV-B and KΔac-B cells is shown below. The band corresponding to KΔac overexpressed protein is indicated by an arrow. An unspecific band with higher mobility is detected in EV-B and KΔac-B cells. **B**- Representative images of desmoplakin immunodetection and nuclei staining with Hoechst of EV-B and KΔac-B cells. Scale bar = 100 μm. White dotted lines demarcate syncytial-like structures. The insets show a magnified image of the boxed regions. The bar graph shows the mean ± SEM of the cell fusion index in KΔac-B cells relative to the spontaneous fusion of the control (EV-B) set as 1 (*$p < 0.05$, one sample *t*-test, n = 3). **C**- Protein expression of β-hCG and syncytin-1 in KΔac-B and EV-B. The bar graphs show the mean ± SEM of the densitometric quantification of protein levels normalized to α-tubulin or β-actin relative to expression in EV-B (*$p < 0.05$, one sample *t*-test, n = 3). **D**- Protein expression of KLF6 and KΔac in KLF6-B cells transduced or not with pLenti-EV or pLenti-KΔac virus particles as indicated. The bar graph shows the mean ± SEM of the relative fusion index of KLF6-B in the absence or presence of KΔac protein relative to EV-B. (*$p < 0.05$ *vs* EV-B,±$p < 0.05$ *vs* KLF6-B, ANOVA, Dunnett's multiple comparison test, n = 3).

participate in different stages of the biochemical or morphological differentiation process. Importantly, KLF6 has been shown to be an early response in carcinogenesis [42], wound healing [43], fibrosis [44], differentiation of pre-adipocytes to adipocytes [45], endothelial denudation [46], and in trophoblast differentiation where KLF6 expression rises 2 h after BeWo treatment with forskolin and 2 h after seeding vCTBs [21,22]. This early peak precedes cell fusion and β-hCG expression; and would be responsible for inducing the transcription of genes necessary for trophoblast differentiation.

Trophoblastic cells have a high proliferative capacity, which decreases as differentiation progresses, like in other cell types [47,48]. Here, we show that KLF6 overexpression decreases cell proliferation and raises p21 expression. These data agree with our previous report showing increased p21 levels during vCTB syncytialization and forskolin-treated BeWo cells [22]. Upregulation of p21 was also reported in cell fusion induced by the *ENV* gene of human endogenous retrovirus-3 or with TGFβ1 [49,50]. Interestingly, one of the mechanisms described by which KLF6 inhibits cell growth is the transcriptional

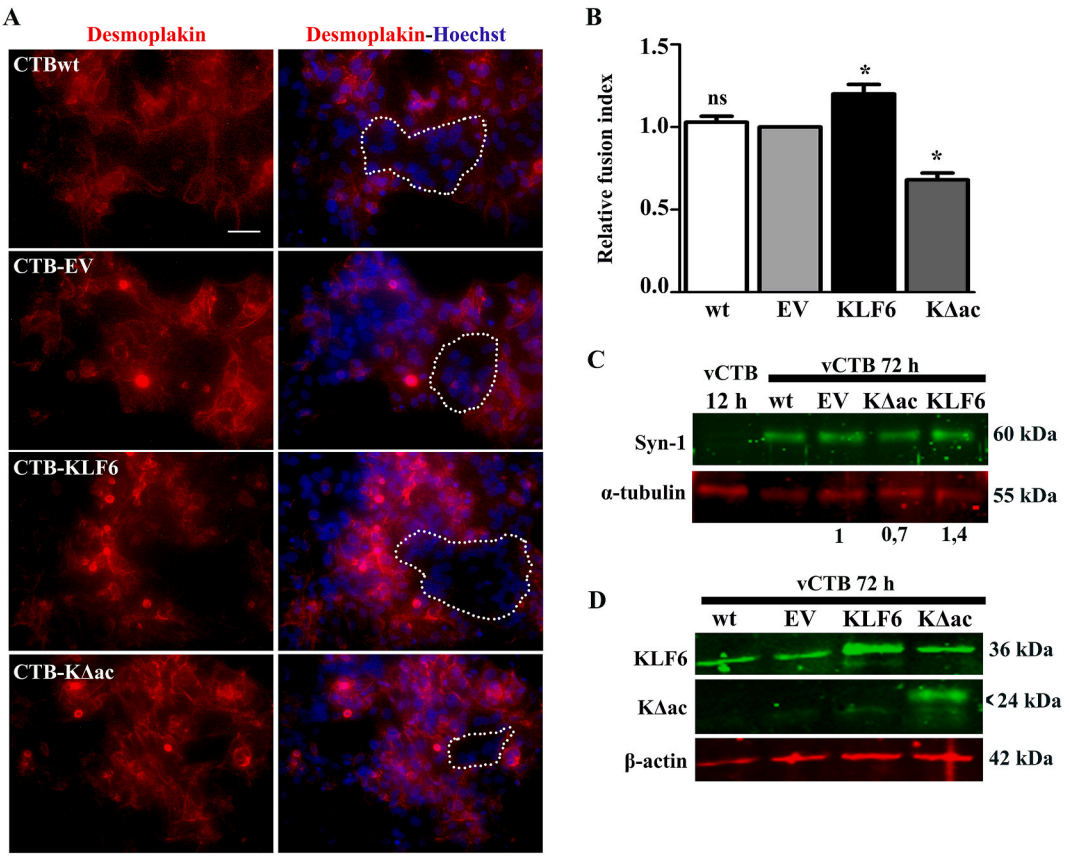

Fig. 6. vCTB syncytialization is promoted by full-length KLF6 and hindered by KLF6 lacking the N-terminal regulatory domain. **A**- Representative images of desmoplakin (red) and nuclei (Hoechst, blue) staining of vCTB primary cell cultures that were untreated (wt) or transduced with the empty vector (EV), KLF6 or KΔac viral particles. The dotted lines delimit syncytial structures. Scale bar = 100 μm. **B**- Fusion index of vCTB cells in the indicated conditions relative to the fusion index of the EV-CTB cells defined as 1. The mean ± SEM is shown (*$p < 0.05$; n = 3, ANOVA, post-test Tukey's multiple comparison, ns: not significant). **C**- Syn-1 protein level measured by western blot in vCTB cells maintained for 12 h (vCTB C12h) and in vCTB cells untreated or transduced with the EV, KLF6 or KΔac viral particles 72 h after plating. The values of the densitometric quantification normalized to the loading control (α-tubulin) relative to the level in EV-CTB are shown. **D**- KLF6 and KΔac proteins expression in the corresponding transduced cells confirmed by western blot analysis. (For interpretation of the references to colour in this figure legend, the reader is referred to the Web version of this article.)

activation of *TGFβ1* and *CDKN1A* genes [23,41,51]. Herein, p21 silencing in KLF6-B cells reduced the cell-cell fusion induced by KLF6. Several reports have shown that p21 is involved in normal and tumor cell differentiation with opposing effects depending on its expression level, post-translational modifications, and cellular microenvironment among other factors [52]. In the placenta, trophoblast syncytialization requires cell cycle arrest and it depends, at least in part, on the expression of p21, which interacts with GCM1 activating the expression of the fusogenic protein Syn-2 [37]. Therefore, present results are consistent with the participation of KLF6 as an inducer of vCTB fusion, at least in part, by increasing p21 expression.

AFM analysis revealed small topography differences but a decreased elasticity in BeWo cells transformed with KLF6. Only few data on trophoblast cell elasticity have been published. They demonstrate Young's Modulus increases in porcine trophoblast stem-like cells and mouse trophoblast stem cells upon differentiation [53,54]. Increased stiffness is widely reported in stem cell differentiation [55–57]. Our results agree with these reports since KLF6 overexpression increased BeWo cell stiffness and fusion.

Herein, we report the first Raman biochemical signature of BeWo cells. PCA analyses revealed a slight increase in the 1101 cm^{-1} peak and a reduction in the intensity of the 1679 cm^{-1} peak in mononuclear cells of the KLF6 group compared to control. The 1101 cm^{-1} peak is associated to the PO2 stretch of DNA, particularly useful to determine the structure of DNA [58]. This suggests KLF6 could induce conformational changes in DNA structure before cell differentiation. Intensity of the 1679 cm^{-1} peak, assigned to amide I and NADH, was reduced in mononucleated as well as in fused cells transduced with KLF6, suggesting protein structure modifications and reduced NADH amount in the presence of KLF6. Interestingly, NADH is involved in multiple enzymatic activities and the NAD(H) redox couple plays crucial roles in maintaining cellular redox state and regulating cellular metabolism [59]. Moreover, NADH has been proposed as an inhibitor of sirtuin-1 [60], that is required for proper trophoblast differentiation and placental development [61]. Future work investigating the role of KLF6 on NADH/NAD balance might prove important for further comprehension of the biochemical control of trophoblast differentiation.

The high fusogenic capacity of KLF6-B cells was accompanied by an increase in GRP78 expression. Interestingly, GRP78 participates in BeWo and vCTB cell differentiation; moreover, the unfolded protein response is not only activated but appears as a trigger for BeWo syncytialization [13,14]. Therefore, KLF6 could induce BeWo cell differentiation in part by activating UPR through the GRP78 chaperone.

The effect of KLF6 on cellular processes is carried out mainly through the activation or repression of target genes [40]. Its regulatory function requires the DNA-binding domain and the amino-terminal acidic domain. Present results show that KΔac reduces the fusion index of human vCTB and BeWo cells, the expression of syncytin-1 and β-hCG, and the fusogenic capacity of the KLF6-B cells, indicating that KLF6 requires its transcriptional regulatory domain to promote vCTB differentiation. The results suggest that KΔac could act as a negative dominant by blocking KLF6 recognition sites in target genes preventing their

regulation by wild-type endogenous KLF6.

Overall, present results support that KLF6 not only participates but is a key transcription factor that triggers villous trophoblast syncytialization through its classic function as a transcription factor in a p21-dependent manner.

Funding

This work was supported by grants from the Agencia Nacional de Promoción Científica y Tecnológica (FONCYT) PICT 2014-0806, 2015-1781, and 2017-0899; and the Secretaría de Ciencia y Técnica de la Universidad Nacional de Córdoba (SECyT-UNC) 05/C479. The funders had no role in study design, data collection and analysis, decision to publish, or preparation of the manuscript.

Author contributions

Conceived and designed the experiments: ALM, ACR and GMP-D. Performed the experiments: ALM, ACR, LTK, MLR, MCDP, GRL, ALXM, STS, ECOS and EJSF. Analyzed the data: ALM, ACR, LTK, MLR, MCDP, ALXM, ECOS, EJSF, SG-R, AUB and GMP-D. Contributed reagents/materials/analysis tools: SG-R, AUB and GMP-D. Provided human placentas with the corresponding ethics statements: AVS and CT. Wrote the paper: ALM, GMP-D. Reviewed the draft article critically: ALM, ACR, LTK, MLR, MCDP, SG-R, AUB and GMP-D. Approved the final manuscript: all authors.

Declarations of competing interest

None.

Acknowledgements

We gratefully acknowledge Dr. Luciana Reyna for molecular biology assistance, Dr. Paula Abadie, Dr. Pilar Crespo and Dr. Estefania Zacca for microscopy and cytometry technical assistance, and Dr. Gabriela Furlan, Dr. Laura Gatica and Camilla Gonçalves for their eukaryotic cell culture assistance. ALM, LTK, MCDP and MLR thank CONICET for their fellowships. ACR, SG-R, and GMP-D are Career Investigators of the Consejo Nacional de Investigaciones Científicas y Técnicas (CONICET).

Appendix A. Supplementary data

Supplementary data to this article can be found online at https://doi.org/10.1016/j.placenta.2021.12.006.

References

[1] B. Huppertz, M. Gauster, Trophoblast fusion, Adv. Exp. Med. Biol. 713 (2011) 81–95, https://doi.org/10.1007/978-94-007-0763-4_6.
[2] G.J. Burton, A.L. Fowden, K.L. Thornburg, Placental origins of chronic disease, Physiol. Rev. 96 (4) (2016) 1509–1565, https://doi.org/10.1152/physrev.00029.2015.
[3] C.S. Roland, J. Hu, C.-E. Ren, H. Chen, J. Li, M.S. Varvoutis, L.W. Leaphart, D. B. Byck, X. Zhu, S.-W. Jiang, Morphological changes of placental syncytium and their implications for the pathogenesis of preeclampsia, Cell. Mol. Life Sci. 73 (2) (2016) 365–376, https://doi.org/10.1007/s00018-015-2069-x.
[4] F. Staud, R. Karahod, Trophoblast: the central unit of fetal growth, protection and programming, Int. J. Biochem. Cell Biol. 105 (2018) 35–40, https://doi.org/10.1016/j.biocel.2018.09.016.
[5] A. Vargas, C. Toufaily, Frédérique LeBellego, É. Rassart, J. Lafond, B. Barbeau, Reduced expression of both syncytin 1 and syncytin 2 correlates with severity of preeclampsia, Reprod. Sci. 18 (11) (2011) 1085–1091, https://doi.org/10.1177/1933719111404608.
[6] G. Daoud, M. Amyot, E. Rassart, A. Masse, L. Simoneau, J. Lafond, ERK1/2 and p38 regulate trophoblasts differentiation in human term placenta, J. Physiol. 566 (2) (2005) 409–423, https://doi.org/10.1113/jphysiol.2005.089326.
[7] A. Gerbaud, A. Pidoux, Review: an overview of molecular events occurring in human trophoblast fusion, Placenta 36 (S1) (2015) S35–S42, https://doi.org/10.1016/j.placenta.2014.12.015.
[8] C.-P. Chen, L.-F. Chen, S.-R. Yang, C.-Y. Chen, C.-C. Ko, G.-D. Chang, H. Chen, Functional characterization of the human placental fusogenic membrane protein syncytin 2, Biol. Reprod. 79 (5) (2008) 815–823, https://doi.org/10.1095/biolreprod.108.069765.
[9] J.-L. Frendo, D. Olivier, V. Cheynet, J.-L. Blond, O. Bouton, M. Vidaud, M. Rabreau, D. Evain-Brion, F. Mallet, Direct involvement of HERV-W env glycoprotein in human trophoblast cell fusion and differentiation, Mol. Cell Biol. 23 (10) (2003) 3566–3574, https://doi.org/10.1128/mcb.23.10.3566-3574.2003.
[10] B. Soygur, L. Sati, The role of syncytins in human reproduction and reproductive organ cancers, Reproduction 152 (5) (2016) 167–178, https://doi.org/10.1530/REP-16-0031.
[11] L.A. Cole, hCG, the wonder of today's science, Reprod. Biol. Endocrinol. 10 (24) (2012), https://doi.org/10.1186/1477-7827-10-24.
[12] M. Yang, M. Lei, C.V. Rao, The central role of human chorionic gonadotropin in the formation of human placental syncytium, Endocrinology 144 (3) (2003) 1108–1120, https://doi.org/10.1210/en.2002-220922.
[13] S. Fradet, S. Pierredon, P. Ribaux, M. Epiney, K. Ya, O. Irion, M. Cohen, Involvement of membrane grp78 in trophoblastic cell fusion, PLoS One 7 (8) (2012) 1–7, https://doi.org/10.1371/journal.pone.0040596.
[14] D. Bastida-Ruiz, L. Yart, C. Wuillemin, P. Ribaux, N. Morris, M. Epiney, B. Martinez de Tejada, M. Cohen, The fine-tuning of endoplasmic reticulum stress response and autophagy activation during trophoblast syncytialization, Cell Death Dis. 10 (9) (2019) 651, https://doi.org/10.1038/s41419-019-1905-6.
[15] D.A. Evseenko, J.W. Paxton, J.A. Keelan, The xenobiotic transporter ABCG2 plays a novel role in differentiation of trophoblast-like BeWo cells, Placenta 21 (28) (2007) 116–120, https://doi.org/10.1016/j.placenta.2006.12.003.
[16] C. Toudic, X. Elisseeff, A. Vargas, Y. Xiao, E. Rassart, J. Lafond, S. Sato, B. Barbeau, Trophoblast fusion is induced by galectin-1 and involves the human endogenous retroviral protein, Placenta 57 (2017) 301–302, https://doi.org/10.1016/j.placenta.2017.07.246.
[17] K.J. Baines, S.J. Renaud, Transcription factors that regulate trophoblast development and function, Prog Mol Biol Transl Sci 145 (2017) 39–88, https://doi.org/10.1016/bs.pmbts.2016.12.003.
[18] M.A. Costa, Scrutinising the regulators of syncytialization and their expression in pregnancy-related conditions, Mol. Cell. Endocrinol. 420 (2016) 180–193, https://doi.org/10.1016/j.mce.2015.11.010.
[19] N.P. Koritschoner, J.L. Bocco, G.M. Panzetta-Dutari, C.I. Dumur, A. Flury, L. C. Patrito, A novel human zinc finger protein that interacts with the core promoter element of a TATA box-less gene, J. Biol. Chem. 272 (14) (1997) 9573–9580, https://doi.org/10.1074/jbc.272.14.9573.
[20] N. Matsumoto, A. Kubo, H. Liu, K. Akita, F. Laub, F. Ramirez, G. Keller, S. L. Friedman, Developmental regulation of yolk sac hematopoiesis by Krüppel-like factor 6, Blood 107 (4) (2006) 1357–1365, https://doi.org/10.1182/blood-2005-05-1916.
[21] A.C. Racca, S.A. Camolotto, M.E. Ridano, J.L. Bocco, S. Genti-Raimondi, G. M. Panzetta-Dutari, Krüppel-like factor 6 expression changes during trophoblast syncytialization and transactivates ßhCG and PSG placental genes, PLoS One 6 (7) (2011), https://doi.org/10.1371/journal.pone.0022438.
[22] A.C. Racca, M.E. Ridano, S. Camolotto, S. Genti-Raimondi, G.M. Panzetta-Dutari, A novel regulator of human villous trophoblast fusion: the Krüppel-like factor 6, Mol. Hum. Reprod. 21 (4) (2015) 347–358, https://doi.org/10.1093/molehr/gau113.
[23] D.A. Slavin, N.P. Koritschoner, C.C. Prieto, F.J. López-Díaz, B. Chatton, J.L. Bocco, A new role for the Krüppel-like transcription factor KLF6 as an inhibitor of c-Jun proto-oncoprotein function, Oncogene 23 (50) (2004) 8196–8205, https://doi.org/10.1038/sj.onc.1208020.
[24] M. Vatish, L. Tesfa, D. Grammatopoulos, E. Yamada, C.C. Bastie, J.E. Pessin, Inhibition of akt activity and calcium channel function coordinately drive cell-cell fusion in the BeWo choriocarcinoma placental cell line, PLoS One 7 (1) (2012), https://doi.org/10.1371/journal.pone.0029353.
[25] R.C. Gehrau, D.S. D'Astolfo, C.I. Dumur, J.L. Bocco, N.P. Koritschoner, Nuclear expression of KLF6 tumor suppressor factor is highly associated with overexpression of ERBB2 oncoprotein in ductal breast carcinomas, PLoS One 5 (1) (2010), e8929, https://doi.org/10.1371/journal.pone.0008929.
[26] M.E. Ridano, A.C. Racca, J.B. Flores-Martín, L. Reyna, S. Genti-Raimondi, G. M. Panzetta-Dutari, Effect of Chlorpyrifos on human extravillous-like trophoblast cells, Reprod. Toxicol. 90 (2019) 118–125, https://doi.org/10.1016/j.reprotox.2019.09.001.
[27] R.M. Botelho, L.P.G. Tenorio, A.L.M. Silva, E.L.L. Tanabe, K.S.N. Pires, C. M. Gonçalves, J.C. Santos, A.L.X. Marques, M.J. Allard, J.D. Bergeron, G. Sebire, E. C.O. Silva, S.T. Souza, E.J.S. Fonseca, A.U. Borbely, K.S.C. Borbely, Biomechanical and functional properties of trophoblast cells exposed to group B Streptococcus in vitro and the beneficial effects of uvaol treatment, Biochim. Biophys. Acta Gen. Subj. 1863 (9) (2019) 1417–1428, https://doi.org/10.1016/j.bbagen.2019.06.012.
[28] T. Etcheverry, P. Accialini, M. Palligas, F. Loureiro, N. Saraco, N. Martínez, M. Farina, Endocannabinoid signaling impairs syncytialization: using flow cytometry to evaluate forskolin-induced cell fusion, Placenta 103 (2021) 152–155, https://doi.org/10.1016/j.placenta.2020.10.028.
[29] Y. Kudo, C.A. Boyd, H. Kimura, P.R. Cook, C.W. Redman, I.L. Sargent, Quantifying the syncytialisation of human placental trophoblast BeWo cells grown in vitro, Biochim. Biophys. Acta 1640 (1) (2003) 25–31, https://doi.org/10.1016/s0167-4889(03)00004-1.
[30] R.P. Wersto, F.J. Chrest, J.F. Leary, C. Morris, M. Stetler-stevenson, E. Gabrielson, Doublet discrimination in DNA cell-cycle analysis, Cytometry 46 (5) (2001) 296–306, https://doi.org/10.1002/cyto.1171.

[31] Z. Movasaghi, S. Rehman, I.U. Rehman, Raman spectroscopy of biological tissues, Appl. Spectrosc. Rev. 42 (5) (2007) 493–541, https://doi.org/10.1080/05704920701551530.
[32] G. Basar, U. Parlatan, S. Seninak, T. Gûnel, A. Benian, I. Kalelioglu, Investigation of preeclampsia using Raman spectroscopy, Journal of Spectroscopy 27 (2012), https://doi.org/10.1155/2012/376793. ID 376793.
[33] K. Czamara, K. Majzner, M.Z. Pacia, K. Kochan, A. Kaczor, M. Baranska, Raman spectroscopy of lipids: a review, J. Raman Spectrosc. 46 (1) (2015) 4–20.
[34] J. De Gelder, K. De Gussem, P. Vandenabeele, L. Moens, Reference database of Raman spectra of biological molecules, J. Raman Spectrosc. 38 (9) (2007) 1133–1147, https://doi.org/10.1002/jrs.1734.
[35] A.C.S. Talari, Z. Movasaghi, S. Rehman, I. Rehman, Raman spectroscopy of biological tissues, Appl. Spectrosc. Rev. 50 (1) (2015) 46–111, https://doi.org/10.1080/05704928.2014.923902.
[36] K. Brandenburg, U. Seydel, in: J.M. Chalmers, P.R. Griffiths (Eds.), Vibrational Spectroscopy of Carbohydrates and Glycoconjugates. *Handbook Of Vibrational Spectroscopy*, 2006, https://doi.org/10.1002/0470027320.s8205.
[37] X. Lu, R. Wang, C. Zhu, H. Wang, H. Lin, Y. Gu, J. Cross, H. Wang, Fine-tuned and cell-cycle-restricted expression of fusogenic protein syncytin-2 maintains functional placental syncytia, Cell Rep. 21 (5) (2017) 1150–1159, https://doi.org/10.1016/j.celrep.2017.10.019.
[38] S. Benzeno, G. Narla, J. Allina, G.Z. Cheng, H.L. Reeves, M.S. Banck, J.A. Odin, J. A. Diehl, D. Germain, S.L. Friedman, Cyclin-dependent kinase inhibition by the KLF6 tumor suppressor protein through interaction with cyclin D1, Cancer Res. 64 (11) (2004) 3885–3891, https://doi.org/10.1158/0008-5472.
[39] G. Narla, S. Kremer-Tal, N. Matsumoto, X. Zhao, S. Yao, K. Kelley, M. Tarocchi, S. L. Friedman, In vivo regulation of p21 by the Kruppel-like factor 6 tumor-suppressor gene in mouse liver and human hepatocellular carcinoma, Oncogene 26 (30) (2007) 4428–4434.
[40] V. Andreoli, R.C. Gehrau, J.L. Bocco, Biology of kruppel-like factor 6 transcriptional regulator in cell life and death, IUBMB Life 62 (12) (2010) 896–905, https://doi.org/10.1002/iub.396.
[41] S.E. Syafruddin, M.A. Mohtar, W. Fahmi, W. Mohamad, Two sides of the same coin: the roles of KLF6 in physiology and pathophysiology, Biomolecules 10 (10) (2020) 1–22, https://doi.org/10.3390/biom10101378.
[42] S. Kremer-Tal, G. Narla, Y. Chen, E. Hod, A. DiFeo, S. Yea, J.S. Lee, M. Schwartz, S. N. Thung, I.M. Fiel, M. Banck, E. Zimran, S.S. Thorgeirsson, V. Mazzaferro, J. Bruix, J.A. Martignetti, J.M. Llovet, S.L. Friedman, Downregulation of KLF6 is an early event in hepatocarcinogenesis, and stimulates proliferation while reducing differentiation, J. Hepatol. 46 (4) (2007) 645–654, https://doi.org/10.1016/j.jhep.2006.10.012.
[43] A. Lalazar, L. Wong, G. Yamasaki, S.L. Friedman, Early genes induced in hepatic stellate cells during wound healing, Gene 195 (2) (1997) 235–243, https://doi.org/10.1016/S0378-1119(97)00159-5.
[44] V. Ratziu, A. Lalazar, L. Wong, Q. Dang, C. Collins, E. Shaulian, S. Jensen, S. L. Friedman, Zf9, a Kruppel-like transcription factor up-regulated in vivo during early hepatic fibrosis, Proc. Natl. Acad. Sci. U.S.A. 95 (16) (1998) 9500–9505, https://doi.org/10.1073/pnas.95.16.9500.
[45] D. Li, S. Yea, S. Li, Z. Chen, G. Narla, M. Banck, J. Laborda, S. Tan, J.M. Friedman, S.L. Friedman, M.J. Walsh, Krüppel-like factor-6 promotes preadipocyte differentiation through histone deacetylase 3-dependent repression of DLK1, J. Biol. Chem. 280 (29) (2005) 26941–26952, https://doi.org/10.1074/jbc.M500463200.
[46] E. Gallardo-Vara, F.J. Blanco, M. Roqué, S.L. Friedman, T. Suzuki, L.M. Botella, C. Bernabeu, Transcription factor KLF6 upregulates expression of metalloprotease MMP14 and subsequent release of soluble endoglin during vascular injury, Angiogenesis 19 (2) (2016) 155–171, https://doi.org/10.1007/s10456-016-9495-8.
[47] M. Knöfler, S. Haider, L. Saleh, J. Pollheimer, T.K.J.B. Gamage, J. James, Human placenta and trophoblast development: key molecular mechanisms and model systems, Cell. Mol. Life Sci. 76 (18) (2019) 3479–3496, https://doi.org/10.1007/s00018-019-03104-6.
[48] S. Ruijtenberg, S. van den Heuvel, Coordinating cell proliferation and differentiation: antagonism between cell cycle regulators and cell type-specific gene expression, Cell Cycle 15 (2) (2016) 196–212, https://doi.org/10.1080/15384101.2015.1120925.
[49] L. Lin, B. Xu, N.S. Rote, The cellular mechanism by which the human endogenous retrovirus ERV-3 env gene affects proliferation and differentiation in a human placental trophoblast model, BeWo, Placenta 21 (1) (2000) 73–78, https://doi.org/10.1053/plac.1999.0443.
[50] S. Rama, Y. Suresh, A.J. Rao, TGF beta1 induces multiple independent signals to regulate human trophoblastic differentiation: mechanistic insights, Mol. Cell. Endocrinol. 206 (1–2) (2003) 123–136, https://doi.org/10.1016/s0303-7207(03)00202-8.
[51] B.B. McConnell, V.W. Yang, Mammalian Krüppel-like factors in health and diseases, Physiol. Rev. 90 (4) (2010) 1337–1381, https://doi.org/10.1152/physrev.00058.2009.
[52] N.N. Kreis, F. Louwen, J. Yuan, The multifaceted p21 (Cip1/Waf1/CDKN1A) in cell differentiation, migration and cancer therapy, Cancers 11 (9) (2019), https://doi.org/10.3390/cancers11091220.
[53] Q. Li, E. Suasnavas, L. Xiao, S. Heywood, X. Qi, A. Zhou1, S.C. Isom2, Non-invasive measurement of trophoblast cell differentiation, J. Biophot. 8 (2015) 638–645, https://doi.org/10.1002/jbio.201400062.
[54] V.B. Zeldovich, C.H. Clausen, E. Bradford, D.A. Fletcher, E. Maltepe, J.R. Robbins, A.I. Bakardjiev, Placental syncytium forms a biophysical barrier against pathogen invasion, PLoS Pathog. 9 (12) (2013), https://doi.org/10.1371/journal.ppat.1003821.
[55] N.D. Evans, C. Minelli, E. Gentleman, V. LaPointe, S.N. Patankar, M. Kallivretaki, X. Chen, C.J. Roberts, M.M. Stevens, Substrate stiffness affects early differentiation events in embryonic stem cells, Eur. Cell. Mater. 18 (2009) 1–14, https://doi.org/10.22203/ecm.v018a01.
[56] A. Pillarisetti, J.P. Desai, H. Ladjal, A. Schiffmacher, A. Ferreira, C.L. Keefer, Mechanical phenotyping of mouse embryonic stem cells: increase in stiffness with differentiation, Cell. Reprogr. 13 (4) (2011) 371–380, https://doi.org/10.1089/cell.2011.0028.
[57] C. Zhou, D. Zhang, W. Du, J. Zou, X. Li, J. Xie, Substrate mechanics dictate cell-cell communication by gap junctions in stem cells from human apical papilla, Acta Biomater. 107 (2020) 178–193, https://doi.org/10.1016/j.actbio.2020.02.032.
[58] I. Notingher, Raman spectroscopy cell-based biosensors, Sensors 7 (8) (2007) 1343–1358, https://doi.org/10.3390/s7081343.
[59] W. Xiao, R.S. Wang, D.E. Handy, J. Loscalzo, NAD(H) and NADP(H) redox couples and cellular energy metabolism, Antioxidants Redox Signal. 28 (3) (2018) 251–272, https://doi.org/10.1089/ars.2017.7216.
[60] S.J. Lin, E. Ford, M. Haigis, G. Liszt, L. Guarente, Calorie restriction extends yeast life span by lowering the level of NADH, Genes Dev. 18 (1) (2004) 12–16, https://doi.org/10.1101/gad.1164804.
[61] K. Arul Nambi Rajan, M. Khater, F. Soncin, D. Pizzo, M. Moretto-Zita, J. Pham, O. Stus, P. Iyer, V. Tache, L.C. Laurent, M.M. Parast, Sirtuin1 is required for proper trophoblast differentiation and placental development in mice, Placenta 62 (2018) 1–8, https://doi.org/10.1016/j.placenta.2017.12.002.